



Lab on a Chip

Microfluidic electrical impedance assessment of red blood cell mediated microvascular occlusion

Journal:	<i>Lab on a Chip</i>
Manuscript ID	LC-ART-11-2020-001133.R2
Article Type:	Paper
Date Submitted by the Author:	18-Feb-2021
Complete List of Authors:	<p>Man, Yuncheng; Case Western Reserve University, Mechanical and Aerospace Engineering Department Maji, Debnath; Case Western Reserve University An, Ran; Case Western Reserve University, Mechanical and Aerospace Engineering Ahuja, Sanjay; Case Western Reserve University Little, Jane; University of North Carolina at Chapel Hill Suster, Michael; Case Western Reserve University Mohseni, Pedram; Case Western Reserve University Gurkan, Umut; Case Western Reserve University, Mechanical and Aerospace Engineering</p>

SCHOLARONE™
Manuscripts

Microfluidic electrical impedance assessment of red blood cell mediated microvascular occlusion

Yuncheng Man ^{a, 1}, Debnath Maji ^{b, 1}, Ran An ^a, Sanjay P. Ahuja ^c, Jane A. Little ^d, Michael A. Suster ^b,
Pedram Mohseni ^{b, e}, Umut A. Gurkan ^{a, e, f*}

^a Mechanical and Aerospace Engineering Department, Case Western Reserve University, Cleveland, OH 44106, USA

^b Electrical, Computer, and Systems Engineering Department, Case Western Reserve University, Cleveland, OH 44106, USA

^c Division of Hematology and Oncology, Rainbow Babies and Children's Hospital, Case Western Reserve University, Cleveland, OH 44106, USA

^d Division of Hematology and Oncology, UNC Blood Research Center, Department of Medicine, University of North Carolina at Chapel Hill, Chapel Hill, NC 27599, USA

^e Department of Biomedical Engineering, Case Western Reserve University, Cleveland, OH 44106, USA

^f Case Comprehensive Cancer Center, Case Western Reserve University, Cleveland, OH 44106, USA

* Corresponding author:

Umut A. Gurkan, Ph.D.

Warren E. Rupp Associate Professor

Case Western Reserve University

10900 Euclid Ave., Cleveland, OH 44106

Phone: +1 (216) 368-6447

Email: umut@case.edu

Web: <https://engineering.case.edu/profiles/uxg23>

¹ These authors contributed equally.

Keywords: Microfluidics; Impedance; Red blood cell deformability; Microvascular occlusion; Microcirculation; Inherited red cell disorders; Rheology

ABSTRACT

Alterations in the deformability of red blood cells (RBCs), occurring in hemolytic blood disorders such as sickle cell disease (SCD), contributes to vaso-occlusion and disease pathophysiology. There are few functional *in vitro* assays for standardized assessment of RBC mediated microvascular occlusion. Here, we present the design, fabrication, and clinical testing of a novel microfluidic device with embedded capillary network-based micropillar arrays and integrated electrical impedance measurement electrodes to address this need. The micropillar arrays consists of microcapillaries ranging from 12 μm to 3 μm , with each array paired with two sputtered gold electrodes to measure the impedance change of the array before and after sample perfusion through the microfluidic device. We define ‘RBC Occlusion Index’ (ROI) and ‘RBC Electrical Impedance Index’ (REI), which represent the cumulative percentage occlusion and cumulative percentage impedance change, respectively. We demonstrate the promise of this assay in two common red cell disorders, SCD and hereditary spherocytosis. We show that the electrical impedance measurement reflects the microvascular occlusion, where REI significantly correlates with ROI that is obtained via high resolution microscopy imaging of the microcapillary arrays. Further, we show that RBC mediated microvascular occlusion, represented by ROI and REI, associates with clinical treatment outcomes and correlates with *in vivo* hemolytic biomarkers, lactate dehydrogenase (LDH) level and absolute reticulocyte count (ARC) in SCD. Impedance measurement obviates the need for high-resolution imaging enabling future translation of this technology for widespread access, portable and point-of-care use. Our findings suggest that the presented microfluidic design and the integrated electrical impedance measurement provide a reproducible functional test for standardized assessment of RBC mediated microvascular occlusion. This microfluidic assay and the newly defined REI may serve as an *in vitro* therapeutic efficacy benchmark for assessing clinical outcome of emerging RBC modifying targeted and curative therapies.

INTRODUCTION

Red blood cells (RBCs) are inherently flexible, which allows them to swiftly pass through microcapillaries, facilitating oxygen transport to tissues ¹. The exceptional deformational capacity of RBCs is due to their large surface area-to-volume ratio, the integrity and organization of the membrane cytoskeletal protein network, and the low cytoplasmic viscosity ^{2, 3}. Pathological changes may cause significant alterations in one or more of a combination of these factors, and consequently lead to decreased RBC deformability or increased stiffness ^{4, 5}. For example, *Plasmodium falciparum*, an infectious parasite associated with lifelong morbidity and early mortality, significantly reduces host RBC deformability by generating adhesion related antigens and by impairing the elastic properties of the cell membrane ^{6, 7}. In sickle cell disease (SCD), abnormal intracellular polymerization of sickle hemoglobin causes distorted membrane morphology, increased adhesiveness, and decreased cellular deformability ⁸⁻¹⁵. In hereditary spherocytosis (HS), the molecular mutations in the genes encoding RBC cytoskeletal proteins (e.g., spectrin, ankyrin, Band 3, and protein 4.2) result in a number of abnormalities, including loss of membrane surface area, decreased cellular deformability, and defective membrane mechanical stability ¹⁶. RBCs with abnormal deformability and membrane defects may hemolyze in circulation and disrupt normal blood flow, resulting in a range of abnormalities, including anemia, reticulocytosis, vascular inflammation, and microcirculatory occlusion ¹⁷⁻²⁰.

Conventional techniques for RBC deformability assessment, including atomic force microscopy (AFM) ²¹, optical tweezers ²², and micropipette aspiration ^{23, 24}, measure cellular deformability at single-cell level. These methods involve technically challenging procedures that require skilled personnel and specialized equipment. Bulk-cell approaches include shear flow-based and deformation-based techniques. Shear flow-based techniques, including ektacytometry ²⁵⁻²⁸ and microfluidic systems ²⁹⁻³⁶, measure RBC deformability by stretching RBCs under shear flow to obtain their elongation or deformation index via laser diffraction or high-speed camera. Deformation-based methods, including cell transit analyzer ^{37, 38} and other microscale techniques ^{13, 39-50}, infer RBC deformability from the cell's transit time, transit velocity, transit pressure,

wedging, or cell retention rate through capillary networks that are narrower than the RBC. Even though these techniques allow RBC deformability measurements, they can only describe rheological properties of cellular membranes rather than measuring the capacity of RBCs to mechanically deform and pass through microcapillaries. We explored measuring this functional property in this work, which is the vital characteristic of RBCs for traversing the intricate capillary networks in the body to effectively deliver oxygen to the cells and tissues.

The development of a standardized, functional *in vitro* assay for objective and quantitative assessment of RBC mediated microvascular occlusion would contribute to a better understanding of the pathophysiological impact of abnormal RBC deformability on the microcirculation. A physiologically relevant device to assess RBC mediated microvascular occlusion should mimic the key dimensions of microcapillaries (3 μm to 10 μm) observed in the capillary bed⁵¹. Microfluidic designs with microstructures of several micrometers molded in Polydimethylsiloxane (PDMS) elastomers have been realized to partially mimic the capillary bed to investigate the impact of abnormal RBC deformability in malaria and other pathological conditions⁵²⁻⁵⁴. To measure microcapillary occlusion or RBC retention, these earlier techniques employed an experimental procedure that relies on high-resolution optical imaging, which significantly limits their potential for widespread, portable and point-of-care use. The concept of measuring cellular obstruction of capillary networks due to abnormal RBC deformability through electrical impedance readout was recently introduced⁵⁵. The microfluidic design in this study allowed relatively low-throughput processing volume and thus offered limited sampling of RBCs in a blood sample. Pathological RBCs often constitute a small fraction of the entire blood cell population, thus, processing a large number of RBCs is critical in acquiring meaningful results from clinical blood samples, as demonstrated in this study.

Here, we present a standardized, functional *in vitro* microfluidic assay that allows objective and quantitative assessment of RBC mediated microvascular occlusion. To that end, we designed a microfluidic device with embedded micropillar arrays comprising a gradient of narrow microcapillaries from 12 μm down to 3 μm along the flow direction mimicking the non-uniform small blood vessels in the capillary bed. Such design

enabled stiffer RBCs to be retained in the upstream arrays representing larger microcapillaries, while less stiff RBCs were retained in the downstream arrays representing smaller microcapillaries. The upstream array with 12- μm microcapillaries, which does not represent the typical microcapillary dimension in the capillary bed (which are typically less than 10 μm), was included to trap potential large-cell aggregates. Moreover, the micropillar arrays were coupled with two 40- μm -wide side pathways that mimic arteriovenous anastomoses. Anastomoses are bypass passageways around capillary beds, which provide alternative flow paths in the event of blockages in the microcapillaries^{56,57}. These anastomosis-mimicking pathways helped regulate blood flow such that when the upstream portion of an array was saturated, the incoming RBCs could still flow around and into the downstream arrays, which prevented congestion of the microchannel. These features enabled testing of clinical samples at near-hematocrit levels and full utilization of the microcapillary domain. Finally, each micropillar array was paired with two sputtered gold electrodes on the channel bottom surface for electrical impedance measurement. The impedance of each array across the paired electrodes was obtained before and after sample perfusion. We used healthy RBCs, glutaraldehyde-stiffened RBCs, and RBCs from two common red cell disorders, SCD and HS, to validate the microfluidic design and to demonstrate its clinical relevance. We introduced two new parameters, 'RBC Occlusion Index' (ROI) and 'RBC Electrical Impedance Index' (REI), which represent the cumulative percentage occlusion and cumulative percentage impedance change, respectively. We showed that the REI significantly correlates with the ROI, and both ROI and REI associate with *in vivo* hemolytic biomarkers, serum lactate dehydrogenase (LDH) levels and absolute reticulocyte counts (ARCs), as well as treatment outcomes in subjects with SCD. The presented microfluidic device with the integrated electrical impedance measurement, in which the need for high-resolution imaging is obviated, enables future translation of this technology for widespread access and point-of-care use.

METHODS

Concept and design

The microfluidic design comprises capillary network-inspired micropillar arrays and sputtered electrodes paired with each array. As RBCs flow through the microchannel, deformable RBCs are able to clear through, while stiff RBCs are retained within the microcapillaries (Fig. 1A). As a result, the electrical impedance of the micropillar array across the paired electrodes increases in accordance with the resultant occlusion due to the retained RBCs. The microchannel geometry features two key aspects of the human capillary bed: the small capillaries (less than 10 μm) and the arteriovenous anastomoses^{56, 57}. To mimic small capillaries, micropillar arrays were embedded into the microchannel comprising microcapillaries from 12 μm down to 3 μm along the flow direction (Fig. 1B). The micropillars were designed to be 20- μm long, 10- μm wide, and 12- μm tall (Fig. 1B inset), with a column-to-column spacing of 20 μm and array-to-array spacing of 1 mm. This feature enabled less stiff RBCs to be retained by downstream finer microcapillaries while stiffer RBCs were retained by upstream coarse microcapillaries. The near-inlet 12- μm micropillar array was designed to retain large-cell aggregates or contamination that may be present in the blood flow. To mimic the anastomoses around capillary beds, the micropillar arrays were coupled with two 40- μm -wide side pathways (Fig. 1B inset). This feature helped regulate blood flow around the obstructed area to prevent clogging of the microchannel. Moreover, each micropillar array was flanked by a pair of planar gold electrodes for sensing variation of electrical impedance due to retained RBCs (Fig. 1B). Overall, the microchannel is 24-mm long, 4-mm wide, and 12- μm thick.

Device fabrication

The microfluidic device was fabricated using standard soft photolithography protocols. Initially, a master silicon wafer was fabricated by micropatterning a uniform SU8-2010 (Microchem, Newton, MA) photoresist layer. Briefly, the SU8-2010 layer was spin-coated at 2500 rpm over the silicon wafer and soft-baked at 95 °C for 4 min. Next, the wafer was exposed to UV light and post-exposure baked at 95 °C for 4 min. Thereafter, the wafer was developed in 1-methoxy-2-propanol acetate (Sigma Aldrich, St. Louis, MO),

and hard-baked at 110 °C overnight. The master wafer was then used for PDMS casting (10:1 ratio, 80 °C overnight). The PDMS blocks were peeled-off and punched with 0.5 mm-diameter ports for inlets and outlets. Substrate fabrication process started with sonicating standard microscope glass slides with isopropanol for 15 min at room temperature. After drying, multiple gold electrodes with dimensions of 10.5 mm × 0.5 mm with a spacing of 2.5 mm and contact pads with dimensions of 4.5 mm × 4.5 mm were sputter-deposited (150 Å/2000 Å Ti/Au) under a laser-micromachined Kapton tape mask. Thereafter, a layer of amorphous silica (5000 Å/SiO₂) was sputter-deposited under a secondary laser-micromachined Kapton tape mask to ensure proper sealing. All radiofrequency (RF) sputtering processes were performed in Denton Vacuum Explorer 14 System (Moorestown, NJ). Finally, the PDMS block was covalently bonded to the substrate using oxygen plasma. The obtained device was incubated at 60 °C for 30 min on a hotplate to increase the bonding strength. Detailed fabrication process of the substrate is illustrated in Fig. S1. The cross marks were designed to achieve electrode and micropillar array alignment.

Blood sample acquisition and processing

De-identified blood samples were collected in ethylenediaminetetraacetic acid (EDTA)-containing vacutainers from healthy donors or subjects with homozygous (HbSS) SCD or HS at University Hospitals Cleveland Medical Center under Institutional Review Board (IRB)-approved protocols. The obtained blood samples were stored at 4 °C until tested. Signed informed consent forms were obtained from all study participants. RBCs were isolated from the obtained whole blood samples by centrifuging at 500× g for 5 min at room temperature. Plasma, buffy coat, and the near-plasma portion of the RBC pellet were carefully removed. The RBC pellet was then washed twice in phosphate-buffered saline (PBS). Unless otherwise stated, the isolated RBCs were re-suspended in PBS at 20% hematocrit and tested. All experiments were completed within 48 hours of venipuncture in this study. Clinical variables of the study population with SCD are summarized in Table S1.

Glutaraldehyde stiffening of healthy RBCs

In order to validate the microfluidic device functionality of assessing RBC mediated microvascular occlusion, healthy RBCs were isolated and treated with 0.08% w/v glutaraldehyde (Sigma Aldrich) for 10 min at room temperature. The glutaraldehyde-stiffened RBCs were then washed with PBS, mixed with untreated healthy RBCs from the same donor at either 1% or 2% v/v ratio, and re-suspended in PBS at 20% hematocrit for testing. Healthy RBCs from the same healthy donor were included in the study design as control.

Test procedure

Microchannels were initially washed with absolute ethanol (100%) and PBS (1×), which was followed by incubation with 2% bovine serum albumin (BSA) overnight to prevent non-specific binding of RBCs to the channel walls. A Flow-EZ™ microfluidic flow control system (Fluigent, Lowell, MA) was used to regulate the flow (Fig. S2). An impedance analyzer (Agilent 4294A, Santa Clara, CA) coupled with a custom printed-circuit board was used to perform electrical impedance measurements. Briefly, impedance magnitude across each of the 3- μm to 10- μm micropillar arrays was recorded over the frequency range of 40 Hz – 1 MHz before introducing blood into the microchannel and after completing the washing step. Fig. S3 shows the raw impedance data of the 3- μm micropillar array measured for a typical clinical blood sample. For all impedance analyses, a spot frequency of 10 kHz was chosen to minimize potential electrode polarization effects at lower frequencies and avoid parasitic inductances associated with higher frequencies. Hence, data are reported as a percentage change of impedance at 10 kHz in this study.

Prior to the experiment, PBS was perfused through the microchannel at 100 mBar for 15 min to allow for any volumetric changes of the microchannel. Thereafter, the baseline impedance reading was obtained for each micropillar array without stopping the PBS flow. Next, the RBC sample was loaded into the sample reservoir and perfused for 20 min, followed by post-perfusion PBS washing for 20 min. A second impedance reading was then obtained for each micropillar array upon the conclusion of the post-perfusion wash step. The 12- μm micropillar array was excluded from the measurement since it was designed to

prevent large-cell aggregates or contamination, as stated earlier. System background noise was characterized by repeatedly testing PBS (background electrolyte) using five different devices. For select experiments, the electrical impedance of the 3- μm micropillar array was continuously monitored over the entire duration of the experiment.

To determine the association between the electrical impedance change and microcapillary occlusion in the microchannel, an Olympus IX83 inverted motorized microscope with Olympus CellSense live-cell imaging and analysis software were used to obtain high-resolution microscopic images. The images were further processed by Adobe Photoshop software (San Jose, CA), in which the obstructed microcapillaries were manually counted. Typically, it takes less than 45 min to complete the microfluidic processing and electrical impedance data acquisition/analysis for testing one clinical blood sample. The microfluidic device was designed to be single-use and disposable to prevent any cross-contamination between the samples tested. Each data point in this manuscript was generated with a single use of a newly made device.

RBC Occlusion Index and RBC Electrical Impedance Index

To effectively compare the overall microcapillary occlusion and the overall impedance change caused by different RBC samples, we defined ‘RBC Occlusion Index’ (ROI) and ‘RBC Electrical Impedance Index’ (REI) using the following equations,

$$ROI = \sum_i^n \frac{O_i}{N_i} \times 100\% \quad (1)$$

$$REI = \sum_i^n \frac{I_{i2} - I_{i1}}{I_{i1}} \times 100\% \quad (2)$$

Where,

n = Total number of capillary networks within the area of interest

i = The i th capillary network within the area of interest

O_i = The number of microcapillary occlusion in the i th capillary network

$N_i =$ Total number of microcapillaries in the i th capillary network

$I_{i1} =$ The first electrical impedance reading of the i th capillary network

$I_{i2} =$ The second electrical impedance reading of the i th capillary network

Therefore, ROI represents the cumulative percentage occlusion of the capillary networks and REI represents the cumulative percentage impedance change of the capillary networks across the device. The area of interest in our device contains the 3- μ m to 10- μ m micropillar arrays. The upstream 12- μ m array was included to trap potential large-cell aggregates. The concepts of ROI (i.e., the cumulative percentage occlusion of the capillary networks) and REI (i.e., the cumulative percentage impedance change of the capillary networks) are translatable to any microfluidic device employing capillary networks and electrical impedance measurement to assess occlusion/impedance change due to abnormal cellular deformability.

Statistical methods

Data were reported as mean \pm standard deviation (mean \pm SD) in this study. Data were initially analyzed for normality followed by appropriate comparison methods: paired t-test for paired data, one-way ANOVA for normally distributed data, or Mann-Whitney for non-normally distributed data. Linear regression was used to assess the relationship between two variables, and the Pearson correlation coefficient (PCC) was reported. Mean-shift clustering technique^{58,59} was used to categorize the study population with SCD based on their ROI and REI results. A custom-written code in MATLAB (MathWorks, Natick, MA) was utilized for the clustering analysis. Statistical significance was defined with p-value less than 0.05 ($p < 0.05$). All statistical analyses were carried out using Minitab 19 software (Minitab Inc., State College, PA).

RESULTS

Characterization of system background noise

We tested PBS (background electrolyte) using five different devices and found that the resultant electrical impedance changes of individual micropillar arrays ranged from -0.57% to 0.95% (Fig. S4, mean \pm SD = 0.14% \pm 0.33%). The 95% confidence interval was calculated as 0.01–0.27%. Hence, any impedance changes less than 0.27% could be attributed to the system background noise, and were thereby rounded to zero in blood tests.

Validation of the micropillar arrays and the integrated electrical impedance measurement using glutaraldehyde-stiffened RBCs

Glutaraldehyde is a non-specific protein cross-linker, which is commonly used to stiffen RBCs in order to mimic pathologically abnormal RBC deformability⁶⁰⁻⁶². Mild glutaraldehyde stiffening (0.08% w/v in PBS) was applied to RBCs in order to validate the micropillar arrays and the integrated electrical impedance measurement (Fig. 1C and insets). Of note, continuous monitoring of the impedance of the 3- μ m micropillar array with four different samples, including PBS, a sample with 100% healthy RBCs, and a sample with 98% healthy RBCs and 2% stiff RBCs, revealed a unique feature of the presented device: the profile of the impedance change is significantly affected by the presence of healthy RBCs and stiff RBCs in the blood flow (Fig. 1D). In addition, we found that the level of microcapillary occlusion increased as the fraction of the stiff RBCs in the tested RBC samples increased (Fig. 2A). Further, the ROI of samples with 98% healthy RBCs and 2% stiff RBCs was significantly higher compared to that of samples with 99% healthy RBCs and 1% stiff RBCs or 100% healthy RBCs (Fig. 2B, mean \pm SD = 36.16% \pm 4.44% vs. 17.15% \pm 1.78% or 7.61% \pm 1.67% for 2% stiff RBCs vs. 1% stiff RBCs or healthy, $p=0.003$ or $p=0.001$, paired t-test), and the ROI of samples with 99% healthy RBCs and 1% stiff RBCs was significantly higher compared to that of 100% healthy RBCs (Fig. 2B, $p=0.010$, paired t-test). Notably, we observed that magnitude of impedance variation also increased as the fraction of the stiff RBCs in the tested RBC samples increased (Fig. 2C). Moreover, the REI of samples with 98% healthy RBCs and 2% stiff RBCs was significantly higher

compared to that of samples with 99% healthy RBCs and 1% stiff RBCs or 100% healthy RBCs (Fig. 2D, mean \pm SD = 20.99% \pm 1.42% vs. 9.40% \pm 1.61% or 4.35% \pm 1.44% for 2% stiff RBCs vs. 1% stiff RBCs or healthy, $p=0.002$ or $p<0.001$, paired t-test), and the REI of samples with 99% healthy RBCs and 1% stiff RBCs was significantly higher compared to that of 100% healthy RBCs (Fig. 2D, $p=0.013$, paired t-test). Importantly, our results reveal that REI significantly correlates with ROI in these tests (Fig. 2E, $PCC=0.987$, $p<0.0001$, $N=12$).

Validation of the process repeatability and reproducibility of results

To validate the process repeatability and reproducibility of results, we tested one RBC sample obtained from a single healthy donor using five devices manufactured from different batches. The results were highly consistent, where the ROI of the sample is 9.03% \pm 0.89%, and the REI of the sample is 5.42% \pm 1.29% (Fig. 3, mean \pm SD).

Assessments of RBC mediated microvascular occlusion in sickle cell disease and hereditary spherocytosis

To demonstrate the clinical relevance of the present microfluidic device and the integrated electrical impedance measurement, we tested clinical samples from 12 subjects with homozygous (HbSS) SCD and 2 subjects with HS and compared the results with samples from 5 health donors. We found that the level of microcapillary occlusion increased when comparing RBCs from subjects with SCD or HS to RBCs from healthy donors (Fig. 4A). Further, the ROI of RBCs from subjects with SCD or HS is significantly higher compared to that of RBCs from healthy donors (Fig. 4B, mean \pm SD = 34.65% \pm 21.99% or 23.46% \pm 2.55% vs. 8.02% \pm 1.71% for SCD or HS vs. healthy, $p=0.018$ or $p<0.001$, one-way ANOVA). Notably, magnitude of impedance variation also increased when comparing RBCs from subjects with SCD or HS to RBCs from healthy donors (Fig. 4C). Moreover, the REI of RBCs from subjects with SCD or HS is

significantly higher compared to that of RBCs from healthy donors (Fig. 4D, mean \pm SD = 14.93% \pm 10.48% or 11.17% \pm 1.14% vs. 4.31% \pm 1.25% for SCD or HS vs. healthy, $p=0.043$ or $p=0.001$, one-way ANOVA). Further, our results indicate that REI significantly correlates with ROI in these tests (Fig. 4E, PCC=0.946, $p<0.0001$, N=19).

RBC mediated microvascular occlusion and the resultant ROI and REI correlate with clinical hemolytic biomarkers in sickle cell disease

We next explored whether the clinical phenotypes of the study population with SCD affected microvascular occlusion. We found that ROI and REI significantly associated with *in vivo* biomarkers of hemolysis, including serum LDH levels (Fig. S5A, PCC=0.814, $p=0.001$) and ARCs (Fig. S5B, PCC=0.582, $p=0.047$) in the study population with SCD. Next, we assessed whether the electrical impedance change is associated with these biomarkers. Our results indicate that the REI significantly correlates with serum LDH levels (Fig. S5C, PCC=0.698, $p=0.012$) and ARCs (Fig. S5D, PCC=0.731, $p=0.007$) in the study subjects with SCD.

ROI and REI as an *in vitro* therapeutic benchmark to assess clinical outcome of treatments in SCD

We further assessed whether treatments of the study population with SCD affected microvascular occlusion. We performed mean-shift clustering analysis and identified a sub-group of subjects (Group 1, N=5) with distinct ROI and REI profiles compared to the rest (Group 2, N=7, Fig. 5A). We found that Group 1 subjects had significantly lower levels of ROI (Fig. 5B, mean \pm SD = 13.42 \pm 4.57% vs. 49.81 \pm 15.13%, $p<0.001$, one-way ANOVA) and REI (Fig. 5C, mean \pm SD = 4.84 \pm 1.39% vs. 22.13 \pm 7.40%, $p=0.006$, Mann-Whitney) compared to Group 2 subjects. We then determined that among the five Group 1 subjects who had less severe microvascular occlusion, one received allogeneic hematopoietic stem-cell transplantation (HSCT), one was on-hydroxyurea (HU), and the other three were on-transfusion (Fig. 5A). We next

explored whether the two groups of subjects differ in terms of other clinical variables. Accordingly, we found that Group 1 subjects had relatively lower serum LDH levels (Fig. 5D, 242 ± 53 vs. 339 ± 105 U/L, $p=0.052$, Mann-Whitney) and significantly higher ARC levels (Fig. 5E, mean \pm SD = 209 ± 136 vs. 412 ± 192 10^9 /L, $p=0.037$, Mann-Whitney) compared to Group 2 subjects. Comparison of clinical variables between the two groups is summarized in Table S2.

DISCUSSION

Results reported in this study suggest that the presented microfluidic device and the integrated electrical impedance measurement provide a functional, reproducible *in vitro* approach for assessing microvascular occlusion associated with abnormal RBC deformability. Glutaraldehyde is a non-specific protein cross-linker, which is commonly used to verify new RBC deformability measurement techniques⁶². Our results on glutaraldehyde-stiffened RBCs suggest that the present microfluidic assay is deformability-based and is able to discriminate different RBC samples with 1% variation in the fraction of stiff RBCs over the entire RBC population (Fig. 2B&D). However, the RBC deformability resulting from glutaraldehyde stiffening is not comparable to that of pathological RBCs in red cell disorders. Therefore, we further validated the microfluidic device with samples from people with RBC disorders, namely, SCD and HS. HS, mostly prevalent among northern Europeans, results in a fragile RBC membrane^{53,63}. We found that RBCs in two subjects with HS were less deformable, as reflected by a higher ROI and REI compared to healthy RBCs (Fig. 4B&D). SCD, prevalent in the African diaspora, is one of the most common inherited blood disorders worldwide and affects millions of people with considerable morbidity and mortality⁶⁴⁻⁶⁷. Both the abnormal RBC deformability and the molecular basis of SCD are well established in SCD^{68,69}. In accordance with previous studies, we found that the ROI and REI of RBCs from people with SCD were significantly higher, therefore less deformable, compared to RBCs from control subjects (Fig. 4B&D). Interestingly, our results show that RBCs from people with SCD had relatively higher ROI and REI compared to those from the two subjects with HS (Fig. 4B&D). An early study using isotonic ektacytometry revealed that reduction in

isotonic RBC deformability is higher in SCD than in HS⁷⁰. We postulate that these observations are due to the fact that pathological RBCs from different diseases are affected to different extents.

Electrical measurement is widely adopted in numerous microfluidic designs for biological sample testing, largely due to its simplicity, efficiency, and its potential for adaptation for point-of-care tests^{64, 71-78}. We have recently developed a novel microfluidic platform, termed OcclusionChip, for assessing RBC mediated microvascular occlusion in one of our previous studies⁷⁹. Compared to the OcclusionChip, the presented microfluidic design has a micropillar array in the downstream with narrower microcapillaries (3 μm compared to 4 μm). This feature may improve the sensitivity of this test for disease in which a subtle fraction of RBCs are abnormal. Flow rate is a key parameter that could affect the measurement. The flow rate here is mediated by inlet pressure, medium viscosity (dominated by hematocrit⁶⁷), and microchannel flow resistance. For standardized microfluidic assessment, we employed a digital microfluidic pressure pump to allow a constant inlet pressure, and also carefully adjusted the hematocrit value of RBC suspension at 20% for all the tested samples. Further, the microchannel is 12- μm thick, which is larger than the thickness of RBCs ($\sim 2 \mu\text{m}$). Hence, when RBCs are retained in the microcapillaries, other cells are still able to transit through the microcapillaries (as evidenced in Video S1). This feature, along with the large scale of the micropillar arrays and the two 40- μm -wide side passageways (anastomoses), make the microfluidic system hard to saturate, largely preventing a potential build-up of flow resistance in the microchannel due to RBC retention. Moreover, the total volume of the blood sample processed within one testing cycle was measured as approximately 40 μL , which translates to a processing rate of 4 million RBCs/min (with an estimated blood density of 1.06 g/mL⁸⁰ and 2 million RBCs/ μL of blood at 20% hematocrit⁸¹). Such high volume-processing throughput of our device ensures meaningful test results with clinical blood samples.

The microfluidic device was integrated with surface electrodes for electrical impedance measurement capabilities, and the REI measurements significantly correlate with ROI measurements (Fig. 2E and Fig. 3E), suggesting that REI could serve as a robust indicator of the overall microcapillary occlusion across the

device, and that the integrated electrical impedance measurement could replace high-resolution imaging when applying the device in primary healthcare settings. The microfluidic device provides a finer and more rapid detection compared to previous devices, an alternative functional metric for standardized assessments of RBC mediated microvascular occlusion with no need for high-resolution imaging, with the potential to be developed as a truly small-sized, portable device providing real-time results at the point-of-care.

SCD is a clinically heterogeneous disease, as the clinical phenotypes vary considerably from subject to subject^{79, 82, 83}. Here, our results show that both the ROI and REI significantly correlate with two *in vivo* hemolytic biomarkers, serum LDH levels and ARCs (Fig. S5), suggesting that subjects with a more severe intravascular hemolysis are more likely to have RBC-driven microvascular occlusion in SCD. We postulate that two factors may have contributed to these results. Firstly, sickle RBCs have been shown to be vulnerable to mechanical stress and microvesicles shedding-off⁸⁴⁻⁸⁶, which leads to increased hemolysis, reduced membrane surface area-to-volume ratio, and decreased deformability. Secondly, reticulocytes are known to be less deformable compared to mature RBCs, due to their spherical shape with smaller surface area-to-volume ratio, less optimal organization of membrane lipids and proteins, and more viscous cytoplasm with a mass of chromatin granules⁸⁷. The presence of reticulocytosis in a subset of people with SCD, due to hemolytic stress, may contribute to the elevated microcapillary occlusion seen in these studies. Of note, we observed a cluster of subjects who had significantly lower levels of ROI and REI compared to the rest (Fig. 5A, B&C) over the study population with SCD. Among these five subjects, one received Allogeneic HSCT, one was on-hydroxyurea (HU), and the other three were on exchange transfusion (Fig. 5A). We determined that these subjects had less severe RBC mediated microvascular occlusion as measured by the microfluidic system, which was consistent with their relatively lower serum LDH levels and significantly lower ARCs (Fig. 5D&E). Exchange transfusion is one of the main therapeutic treatments in SCD, in which normal RBCs from healthy donors are exchanged with sickle RBCs to dilute the concentration of sickle hemoglobin and sickle RBCs in circulation⁸⁸. However, vaso-occlusive events can still occur in transfused patients due to the remaining and newly made sickle, non-deformable RBCs.

Accordingly, we found that the 8 subjects on transfusion therapy among the study population with SCD had significantly higher ROI and REI compared to healthy donors (Fig. S6). Notably, we did not notice any significant difference when comparing ROI and REI between females and males over the study population (Fig. S7). Together, these analyses demonstrate the promise of the microfluidic assay and the REI as an *in vitro* therapeutic efficacy benchmark to assess clinical outcomes. These tests are likely to significantly benefit the development and assessment of targeted and curative therapies for SCD.

Therapeutic *ex vivo* gene transfer into autologous hematopoietic stem cells, also known as gene therapy, is currently the most promising approach that can repair the fundamental cause of SCD and provide long-term curative treatment for the patients^{89, 90}. The National Heart, Lung, and Blood Institute recently launched the ‘Cure Sickle Cell Initiative’ to keep nourishing the collaborative, patient-focused research environment and to support the further development of gene therapy for treating SCD. Close monitoring of the ability of RBCs to clear microcapillaries in the presented microfluidic device before and after a curative therapy would provide valuable insights into the patient clinical outcome. In particular, discrepant RBC populations may arise in the patient after receiving a curative therapy, at which time it is crucial to discern the heterogeneity in the entire cell population and its effects⁹¹. In this study, we found that one patient with SCD, who received Allogeneic HSCT (Fig. 5A), had similar levels of ROI and REI compared to healthy donors (ROI: 10.08% vs. $8.02 \pm 1.71\%$; REI: 2.44% vs. $4.31 \pm 1.25\%$). Based on our results, we will test whether, following curative therapy, we will see a transition from high to low microcapillary occlusion and electrical impedance as non-sickling RBCs replace sickle RBCs *in vivo*.

SARS-CoV-2, a new RNA coronavirus leading to a global pandemic, is the etiological driver of the clinical syndrome coronavirus disease 2019 (COVID-19)^{92, 93}. The disease is characterized by a number of manifestations including persistent dry cough, shortness of breath, hypoxemia, and fever^{94, 95}. In SCD, COVID-19 may trigger severe acute chest syndrome (ACS) and vaso-occlusive crisis⁹⁶. Since RBCs play an important role in oxygen delivery, it is plausible to suspect that their biophysical properties, such as deformability, are deleteriously altered and thus contribute to congestions of microvessels in COVID-19.

Importantly, a recent study showed that COVID-19 is linked with significantly less deformable RBCs⁹⁷, even though the underlying mechanism is yet to be uncovered. Within the context of COVID-19, we envision that our microfluidic assay and the REI may provide a functional biomarker to supplement the current diagnostic tools for disease assessment and monitoring.

A limitation of this study is that when applying the ROI and REI in other microfluidic capillary networks for assessment of pathological RBC deformability, their absolute values may be affected by experimental parameters such as inlet pressure, duration of sample perfusion, and design of the microfluidic capillary networks. Future studies may prospectively focus on characterizing the intrinsic electrical properties of pathological RBCs from a wider range of red cell disorders, including malaria and thalassemia, which will provide more insights into disease pathophysiology and assist the assessment of RBC mediated microvascular occlusion through electrical impedance measurement.

CONCLUSIONS

In this study, a novel microfluidic device integrated with capillary network-inspired micropillar matrices and electrodes for electrical impedance measurement is presented for standardized assessment of RBC mediated microvascular occlusion. Healthy RBCs, glutaraldehyde-stiffened RBCs, and RBCs from subjects with two red cell disorders, SCD and HS, were used to validate the microfluidic device. Two new highly correlated parameters, ROI and REI, have been defined, which represent the cumulative percentage occlusion and the cumulative percentage impedance change, respectively, across the device. Unique features of the present microfluidic device include processing of clinical blood samples at near-physiologic hematocrit (20%), rapid (less than 5 min) data acquisition and analysis, and REI as an alternative functional metric for occlusion assessment in the absence of high-resolution imaging and as a functional test for microvascular health and disease status monitoring. Future work will focus on adapting the microfluidic device for point-of-care use in resource-limited settings and improving the repeatability of portable analyses when performed by minimally trained personnel in the field. The clinical utility of the microfluidic device

and REI as an *in vitro* therapeutic efficacy benchmark in a larger patient population with a wider range of treatments, including emerging therapies with curative intent, also warrants future investigation.

ACKNOWLEDGEMENTS

This work is supported by National Science Foundation (NSF) Career Award 1552782, National Heart, Lung, and Blood Institute (NHLBI) awards: R01HL133574, U01HL117659, T32HL134622, the Cure Sickle Cell Initiative (OT2HL152643), and American Heart Association 17GRNT33661005 grants. Authors acknowledge with gratitude the contributions of patients and clinicians at University Hospitals Cleveland Medical Center. The authors gratefully acknowledge Laurie Dudik's help on the device substrate fabrication at the Electronics Design Center, Case Western Reserve University.

AUTHOR CONTRIBUTIONS

YM and DM contributed equally to this study. YM, DM, and UAG conceived the project. YM and DM conducted the experiments, collected data, and performed data analyses. YM, DM, RA, MAS, PM and UAG discussed and interpreted data. YM and DM prepared the figures and table and wrote the manuscript. YM, DM, RA, JAL, SPA, MAS, PM and UAG edited the manuscript. SPA provided blood samples from subjects with hereditary spherocytosis at University Hospitals Cleveland Medical Center Rainbow Babies and Children's Hospital. JAL provided blood samples from subjects with sickle cell disease at University Hospitals Cleveland Medical Center Adult Sickle Cell Clinic.

CONFLICT OF INTEREST

A patent application has been filed by Case Western Reserve University for this technology.

REFERENCES

1. M. Diez-Silva, M. Dao, J. Y. Han, C. T. Lim and S. Suresh, *Mrs Bull*, 2010, **35**, 382-388.
2. G. Tomaiuolo, *Biomicrofluidics*, 2014, **8**, 051501.
3. P. Guo and B. M. Fu, *Journal of biomechanical engineering*, 2012, **134**, 041003.
4. P. L. Lacelle, *Semin Hematol*, 1970, **7**, 355-371.
5. N. Mohandas, M. R. Clark, M. S. Jacobs and S. B. Shoheit, *J Clin Invest*, 1980, **66**, 563-573.
6. X. Sisquella, T. Nebl, J. K. Thompson, L. Whitehead, B. M. Malpede, N. D. Salinas, K. Rogers, N. H. Tolia, A. Fleig, J. O'Neill, W. H. Tham, F. David Horgen and A. F. Cowman, *eLife*, 2017, **6**.
7. A. M. Dondorp, P. A. Kager, J. Vreeken and N. J. White, *Parasitol Today*, 2000, **16**, 228-232.
8. Y. Alapan, Y. Matsuyama, J. A. Little and U. A. Gurkan, *Technology*, 2016, **4**, 71-79.
9. R. Huisjes, A. Bogdanova, W. W. van Solinge, R. M. Schiffelers, L. Kaestner and R. van Wijk, *Front Physiol*, 2018, **9**.
10. Y. Alapan, C. Kim, A. Adhikari, K. E. Gray, E. Gurkan-Cavusoglu, J. A. Little and U. A. Gurkan, *Transl Res*, 2016, **173**, 74-91 e78.
11. E. Kucukal, J. A. Little and U. A. Gurkan, *Integr Biol*, 2018, **10**, 194-206.
12. M. Kim, Y. Alapan, A. Adhikari, J. A. Little and U. A. Gurkan, *Microcirculation*, 2017, **24**.
13. M. A. Carden, M. E. Fay, X. Lu, R. G. Mannino, Y. Sakurai, J. C. Ciciliano, C. E. Hansen, S. Chonat, C. H. Joiner, D. K. Wood and W. A. Lam, *Blood*, 2017, **130**, 2654-2663.
14. Y. Qiu, B. Ahn, Y. Sakurai, C. E. Hansen, R. Tran, P. N. Mimche, R. G. Mannino, J. C. Ciciliano, T. J. Lamb, C. H. Joiner, S. F. Ofori-Acquah and W. A. Lam, *Nat Biomed Eng*, 2018, **2**, 453-463.

15. N. Praljak, S. Iram, U. Goreke, G. Singh, A. Hill, U. A. Gurkan and M. J. b. Hinczewski, *bioRxiv*, 2020, DOI: 10.1101/2020.07.01.181545.
16. S. Perrotta, P. G. Gallagher and N. Mohandas, *Lancet*, 2008, **372**, 1411-1426.
17. A. C. Frei, Y. Guo, D. W. Jones, K. A. Pritchard, Jr., K. A. Fagan, N. Hogg and N. J. Wandersee, *Blood*, 2008, **112**, 398-405.
18. L. Da Costa, J. Galimand, O. Fenneteau and N. Mohandas, *Blood reviews*, 2013, **27**, 167-178.
19. D. Manwani and P. S. Frenette, *Blood*, 2013, **122**, 3892-3898.
20. N. A. Beare, S. P. Harding, T. E. Taylor, S. Lewallen and M. E. Molyneux, *The Journal of infectious diseases*, 2009, **199**, 263-271.
21. M. Lekka, M. Fornal, G. Pyka-Fosciak, K. Lebed, B. Wizner, T. Grodzicki and J. Styczen, *Biorheology*, 2005, **42**, 307-317.
22. S. Henon, G. Lenormand, A. Richert and F. Gallet, *Biophys J*, 1999, **76**, 1145-1151.
23. D. Kuzman, S. Svetina, R. E. Waugh and B. Zeks, *Eur Biophys J Biophys*, 2004, **33**, 1-15.
24. E. A. Evans, R. Waugh and L. Melnik, *Biophys J*, 1976, **16**, A167-A167.
25. G. J. Streekstra, J. G. G. Dobbe and A. G. Hoekstra, *Opt Express*, 2010, **18**, 14173-14182.
26. O. K. Baskurt, M. R. Hardeman, M. Uyklu, P. Ulker, M. Cengiz, N. Nemeth, S. Shin, T. Alexy and H. J. Meiselman, *Biorheology*, 2009, **46**, 251-264.
27. E. Llaudet-Planas, J. L. Vives-Corrns, V. Rizzuto, P. Gomez-Ramirez, J. Sevilla Navarro, M. T. Coll Sibina, M. Garcia-Bernal, A. Ruiz Llobet, I. Badell, P. Velasco-Puyo, J. L. Dapena and M. M. Manu-Pereira, *International journal of laboratory hematology*, 2018, **40**, 94-102.
28. M. A. Rab, C. K. Kanne, B. A. van Oirschot, J. F. Bos, M. E. Houwing, M. H. Cnossen, R. Schutgens, G. Pasterkamp, R. van Wijk and V. A. Sheehan, *Blood*, 2018, **132**, 2360-2360.
29. G. Tomaiuolo, M. Barra, V. Preziosi, A. Cassinese, B. Rotoli and S. Guido, *Lab Chip*, 2011, **11**, 449-454.
30. S. S. Lee, Y. Yim, K. H. Ahn and S. J. Lee, *Biomed Microdevices*, 2009, **11**, 1021-1027.

31. P. Guruprasad, R. G. Mannino, C. Caruso, H. Q. Zhang, C. D. Josephson, J. D. Roback and W. A. Lam, *Am J Hematol*, 2019, **94**, 189-199.
32. Y. Zheng, J. Chen, T. Cui, N. Shehata, C. Wang and Y. Sun, *Lab Chip*, 2014, **14**, 577-583.
33. Y. Zheng, M. A. Cachia, J. Ge, Z. S. Xu, C. Wang and Y. Sun, *Lab Chip*, 2015, **15**, 3138-3146.
34. J. C. Cluitmans, V. Chokkalingam, A. M. Janssen, R. Brock, W. T. Huck and G. J. Bosman, *Biomed Res Int*, 2014, 764268.
35. Z. Xu, Y. Zheng, X. Wang, N. Shehata, C. Wang and Y. Sun, *Microsyst Nanoeng*, 2018, **4**, 1-6.
36. S. Sakuma, K. Kuroda, C.-H. D. Tsai, W. Fukui, F. Arai and M. Kaneko, *Lab Chip*, 2014, **14**, 1135-1141.
37. M. Rendell, T. Luu, E. Quinlan, S. Knox, M. Fox, S. Kelly and K. Kahler, *Biochim Biophys Acta*, 1992, **1133**, 293-300.
38. M. Rendell, M. Fox, S. Knox, J. Lastovica, W. Kirchain and H. J. Meiselman, *J Lab Clin Med*, 1991, **117**, 500-504.
39. Y. Zheng, E. Shojaei-Baghini, A. Azad, C. Wang and Y. Sun, *Lab Chip*, 2012, **12**, 2560-2567.
40. A. Adamo, A. Sharei, L. Adamo, B. Lee, S. Mao and K. F. Jensen, *Anal Chem*, 2012, **84**, 6438-6443.
41. H. Bow, I. V. Pivkin, M. Diez-Silva, S. J. Goldfless, M. Dao, J. C. Niles, S. Suresh and J. Han, *Lab Chip*, 2011, **11**, 1065-1073.
42. E. Islamzada, K. Matthews, Q. Guo, A. T. Santoso, S. P. Duffy, M. D. Scott and H. Ma, *Lab Chip*, 2019, **20**, 226-235.
43. J. C. Ciciliano, R. Abbaspour, J. Woodall, C. Wu, M. S. Bakir and W. A. Lam, *Lab Chip*, 2017, **17**, 3804-3816.
44. Q. Guo, S. P. Duffy, K. Matthews, X. Deng, A. T. Santoso, E. Islamzada and H. Ma, *Lab Chip*, 2016, **16**, 645-654.
45. A. T. Santoso, X. Y. Deng, J. H. Lee, K. Matthews, S. P. Duffy, E. Islamzada, S. M. McFaul, M. E. Myrand-Lapierre and H. S. Ma, *Lab Chip*, 2015, **15**, 4451-4460.

46. Q. Guo, S. Park and H. Ma, *Lab Chip*, 2012, **12**, 2687-2695.
47. J. Duez, J. P. Holleran, P. A. Ndour, S. Loganathan, P. Amireault, O. Francais, W. El Nemer, B. Le Pioufle, I. F. Amado, S. Garcia, N. Chartrel, C. Le Van Kim, C. Lavazec, V. M. Avery and P. A. Buffet, *Antimicrobial agents and chemotherapy*, 2015, **59**, 4206-4214.
48. S. A. S. Diakite, P. A. Ndour, V. Brousse, F. Gay, C. Roussel, S. Biligui, M. Dussiot, V. Prendki, T. M. Lopera-Mesa, K. Traore, D. Konate, S. Doumbia, J. Cros, S. Dokmak, R. M. Fairhurst, M. Diakite and P. A. Buffet, *Malaria J*, 2016, **15**, 482.
49. Y. Man, E. Kucukal, R. An, A. Bode, J. A. Little and U. A. Gurkan, *Microcirculation*, 2020, e12662.
50. Q. Guo, S. J. Reiling, P. Rohrbach and H. Ma, *Lab Chip*, 2012, **12**, 1143-1150.
51. P. A. Buffet, I. Safeukui, G. Deplaine, V. Brousse, V. Prendki, M. Thellier, G. D. Turner and O. Mercereau-Puijalon, *Blood*, 2011, **117**, 381-392.
52. J. P. Shelby, J. White, K. Ganesan, P. K. Rathod and D. T. Chiu, *P Natl Acad Sci USA*, 2003, **100**, 14618-14622.
53. J. Picot, P. A. Ndour, S. D. Lefevre, W. El Nemer, H. Tawfik, J. Galimand, L. Da Costa, J. A. Ribeil, M. de Montalembert, V. Brousse, B. Le Pioufle, P. Buffet, C. Le Van Kim and O. Francais, *Am J Hematol*, 2015, **90**, 339-345.
54. E. Du, M. Diez-Silva, G. J. Kato, M. Dao and S. Suresh, *P Natl Acad Sci USA*, 2015, **112**, 1422-1427.
55. Y. Qiang, J. Liu, D. Dieujuste and E. Du, *bioRxiv*, 2020, DOI: 10.1101/2020.07.29.227215.
56. A. G. Hudetz, *Microcirculation*, 1997, **4**, 233-252.
57. J. P. Delaney, *Am J Physiol*, 1969, **216**, 1556-1561.
58. K. G. Derpanis, *Lecture Notes*, 2005, 32.
59. D. Comaniciu and P. Meer, *IEEE Transactions on Pattern Analysis Machine Intelligence*, 2002, **24**, 603-619.

60. A. Pantaleo, E. Ferru, G. Giribaldi, F. Mannu, F. Carta, A. Matte, L. De Franceschi and F. Turrini, *Biochem J*, 2009, **418**, 359-367.
61. A. M. Forsyth, J. D. Wan, W. D. Ristenpart and H. A. Stone, *Microvasc Res*, 2010, **80**, 37-43.
62. J. M. Sosa, N. D. Nielsen, S. M. Vignes, T. G. Chen and S. S. Shevkoplyas, *Clin Hemorheol Micro*, 2014, **57**, 275-289.
63. S. Eber and S. E. Lux, 2004.
64. Y. Alapan, J. A. Little and U. A. Gurkan, *Scientific reports*, 2014, **4**, 7173.
65. O. S. Platt, D. J. Brambilla, W. F. Rosse, P. F. Milner, O. Castro, M. H. Steinberg and P. P. Klug, *The New England journal of medicine*, 1994, **330**, 1639-1644.
66. Y. Man, U. Goreke, E. Kucukal, A. Hill, R. An, S. Liu, A. Bode, A. Solis-Fuentes, L. V. Nayak, J. A. Little and U. A. Gurkan, *Blood cells, molecules & diseases*, 2020, **83**, 102424.
67. E. Kucukal, Y. Man, A. Hill, S. Liu, A. Bode, R. An, J. Kadambi, J. A. Little and U. A. Gurkan, *Am J Hematol*, 2020, 1246-1256.
68. P. Noomuna, M. Risinger, S. Zhou, K. Seu, Y. Man, R. An, D. A. Sheik, J. Wan, J. A. Little, U. A. Gurkan, F. M. Turrini, T. Kalfa and P. S. Low, *Br J Haematol*, 2020, DOI: 10.1111/bjh.16671, 599-609.
69. B. S. Pace, S. F. Ofori-Acquah and K. R. Peterson, *Anemia*, 2012, **2012**, 143594.
70. C. Renoux, M. Faivre, A. Bessaa, L. Da Costa, P. Joly, A. Gauthier and P. Connes, *Sci Rep*, 2019, **9**, 6771.
71. D. Maji, M. A. Suster, E. Kucukal, U. D. S. Sekhon, A. S. Gupta, U. A. Gurkan, E. X. Stavrou and P. Mohseni, *IEEE transactions on biomedical circuits and systems*, 2017, **11**, 1459-1469.
72. D. Maji, L. Nayak, J. Martin, U. D. S. Sekhon, A. Sen Gupta, P. Mohseni, M. A. Suster and S. P. Ahuja, *Haemophilia*, 2019, **25**, 885-892.
73. D. Maji, M. De La Fuente, E. Kucukal, U. D. S. Sekhon, A. H. Schmaier, A. Sen Gupta, U. A. Gurkan, M. T. Nieman, E. X. Stavrou, P. Mohseni and M. A. Suster, *J Thromb Haemost*, 2018, **16**, 2050-2056.

74. J. Liu, Y. Qiang, O. Alvarez and E. Du, *Sensors and actuators. B, Chemical*, 2018, **255**, 2392-2398.
75. Y. Zheng, J. Nguyen, C. Wang and Y. Sun, *Lab Chip*, 2013, **13**, 3275-3283.
76. W. Dou, L. Wang, M. Malhi, H. Liu, Q. Zhao, J. Plakhotnik, Z. Xu, Z. Huang, C. A. Simmons, J. T. Maynes and Y. Sun, *Biosens Bioelectron*, 2021, **175**, 112875.
77. W. Dou, Q. Zhao, M. Malhi, X. Liu, Z. Zhang, L. Wang, S. Masse, K. Nanthakumar, R. Hamilton, J. T. Maynes and Y. Sun, *Biosens Bioelectron*, 2020, **167**, 112468.
78. R. An, D. O. Wipf and A. R. Minerick, *Biomicrofluidics*, 2014, **8**, 021803.
79. Y. Man, E. Kucukal, R. An, Q. Watson, J. Bosch, P. A. Zimmerman, J. A. Little and U. A. Gurkan, *Lab Chip*, 2020.
80. D. J. Vitello, R. M. Ripper, M. R. Fettiplace, G. L. Weinberg and J. M. J. J. o. v. m. Vitello, 2015, **2015**.
81. H. E. Judy and N. B. Price, *Journal of the American Medical Association*, 1958, **167**, 563-566.
82. A. Habara and M. H. Steinberg, *Exp Biol Med (Maywood)*, 2016, **241**, 689-696.
83. E. Kucukal, Y. Man, E. Quinn, N. Tewari, R. An, A. Ilich, N. S. Key, J. A. Little and U. A. Gurkan, *Blood Adv*, 2020, **4**, 3688-3698.
84. M. A. Lizarralde Irigorri, S. El Hoss, V. Brousse, S. D. Lefevre, M. Dussiot, T. Xu, A. R. Ferreira, Y. Lamarre, A. C. Silva Pinto, S. Kashima, C. Lapoumeroulie, D. T. Covas, C. Le Van Kim, Y. Colin, J. Elion, O. Francais, B. Le Pioufle and W. El Nemer, *Lab Chip*, 2018, **18**, 2975-2984.
85. E. Ferru, K. Giger, A. Pantaleo, E. Campanella, J. Grey, K. Ritchie, R. Vono, F. Turrini and P. S. Low, *Blood*, 2011, **117**, 5998-6006.
86. E. Nader, M. Romana and P. Connes, *Frontiers in immunology*, 2020, **11**, 454.
87. L. Xie, Y. Jiang, W. Yao, L. Gu, D. Sun, W. Ka, Z. Wen and S. Chien, *Journal of biomechanics*, 2006, **39**, 530-535.
88. C. D. Josephson, L. L. Su, K. L. Hillyer and C. D. Hillyer, *Transfus Med Rev*, 2007, **21**, 118-133.

89. J. A. Ribeil, S. Hacein-Bey-Abina, E. Payen, A. Magnani, M. Semeraro, E. Magrin, L. Caccavelli, B. Neven, P. Bourget, W. El Nemer, P. Bartolucci, L. Weber, H. Puy, J. F. Meritet, D. Grevent, Y. Beuzard, S. Chretien, T. Lefebvre, R. W. Ross, O. Negre, G. Veres, L. Sandler, S. Soni, M. de Montalembert, S. Blanche, P. Leboulch and M. Cavazzana, *The New England journal of medicine*, 2017, **376**, 848-855.
90. E. B. Esrick and D. E. Bauer, *Semin Hematol*, 2018, **55**, 76-86.
91. S. Demirci, N. Uchida and J. F. Tisdale, *Cytotherapy*, 2018, **20**, 899-910.
92. F. Wu, S. Zhao, B. Yu, Y. M. Chen, W. Wang, Z. G. Song, Y. Hu, Z. W. Tao, J. H. Tian, Y. Y. Pei, M. L. Yuan, Y. L. Zhang, F. H. Dai, Y. Liu, Q. M. Wang, J. J. Zheng, L. Xu, E. C. Holmes and Y. Z. Zhang, *Nature*, 2020, **579**, 265-269.
93. K. Yuki, M. Fujiogi and S. Koutsogiannaki, *Clin Immunol*, 2020, **215**, 108427.
94. J. Herrmann, V. Mori, J. H. T. Bates and B. Suki, *Nat Commun*, 2020, **11**, 4883.
95. T. Thomas, D. Stefanoni, M. Dzieciatkowska, A. Issaian, T. Nemkov, R. C. Hill, R. O. Francis, K. E. Hudson, P. W. Buehler and J. C. Zimring, *J. Proteome. Res.*, 2020, **19**, 4455-4469.
96. E. Nur, A. E. Gaartman, C. F. van Tuijn, M. W. Tang and B. J. Biemond, *Am J Hematol*, 2020, **95**, 725.
97. M. Kubankova, B. Hohberger, J. Hoffmanns, J. Fuerst, M. Hermann, J. Guck and M. Krater, *bioRxiv*, 2021, DOI: 10.1101/2021.02.12.429482.

FIGURES

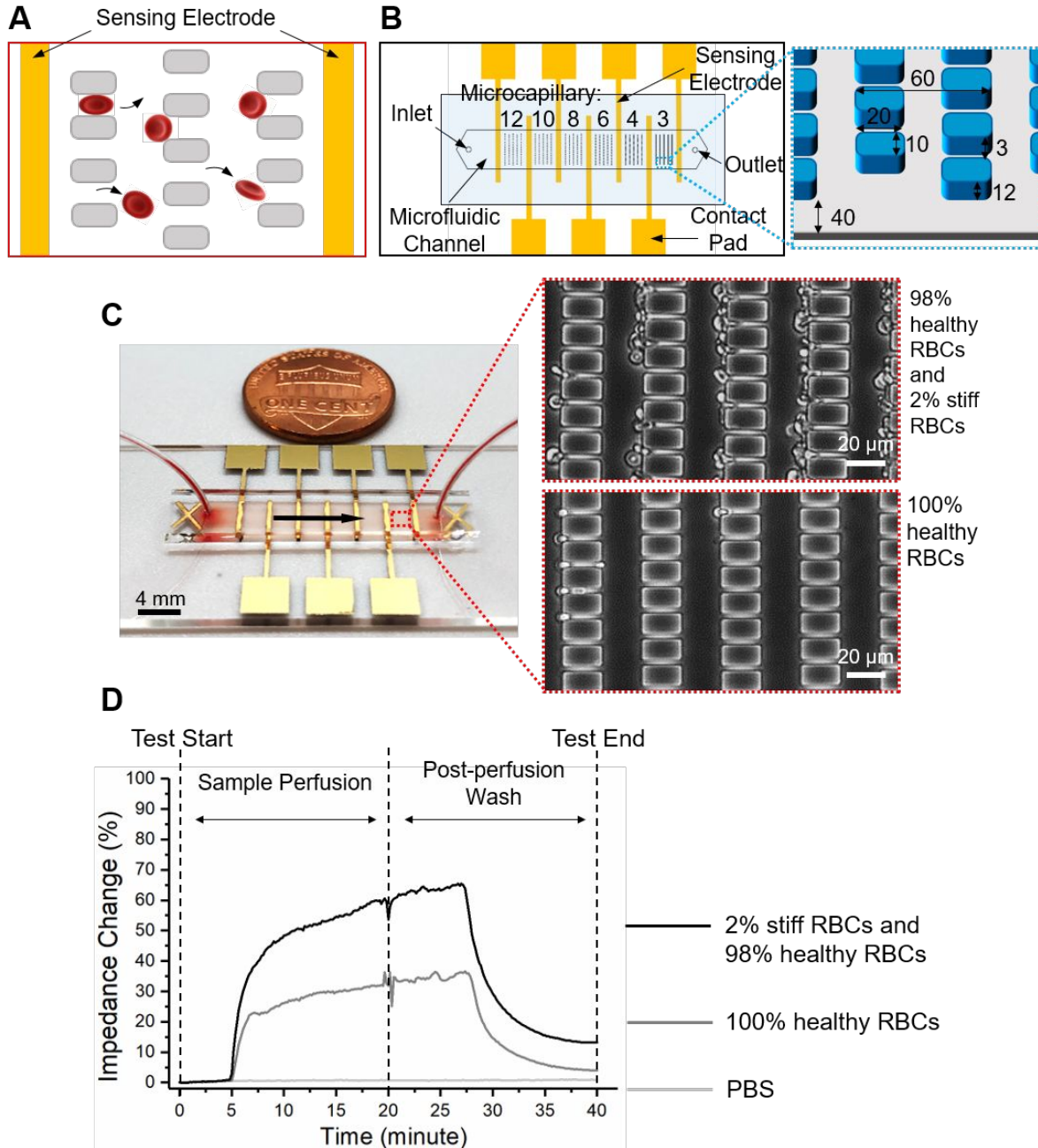


Fig. 1. Microfluidic electrical impedance assessment of RBC mediated microvascular occlusion. (A) Electrical impedance across two electrodes placed on either side of the micropillar array is measured before and after sample perfusion. The resultant impedance change depends on microcapillary occlusion in the array. (B) The microfluidic device consists of six micropillar arrays comprising microcapillaries from 12 μm down to 3 μm , which mimic key dimensions of small blood vessels observed in the capillary bed. The

12- μm array is designed to trap potential large-cell aggregates that may cause microchannel clogging. Inset: Schematic of the capillary-inspired micropillar array. The 40- μm -wide side pathway is designed to mimic arteriovenous anastomoses to help regulate flow and to prevent upstream clogging. Schematics are not drawn to scale, and all dimensions are in microns. (C) Photograph of the microfluidic device is shown. Arrow indicates flow direction. Inset: Close-up views of the microcapillary occlusion within the 3- μm array induced by glutaraldehyde-stiffened RBCs or healthy RBCs. (D) Temporal variation in electrical impedance of the 3- μm array observed at 10 kHz is shown for a sample with 2% stiff RBCs and 98% healthy RBCs, a sample with 100% healthy RBCs, and PBS. Each sample was perfused for 20 min, which was followed by post-perfusion wash with PBS for another 20 min. The initial impedance reading was taken at the start point of each test (Time = 0 min), and the second impedance reading was taken at the endpoint (Time = 40 min).

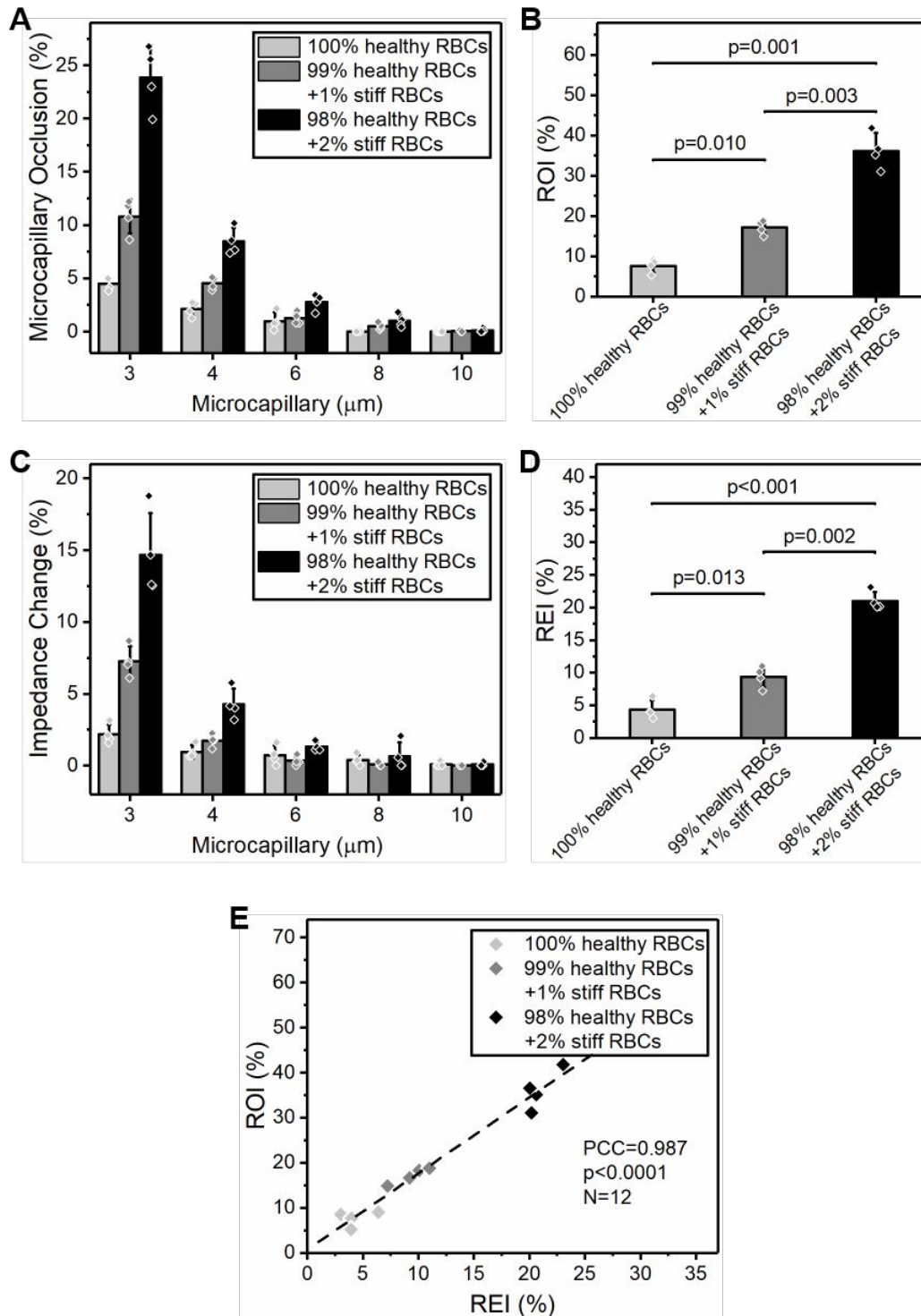


Fig. 2. System characterization using glutaraldehyde-stiffened RBCs (stiff RBCs) and analysis of the microcapillary occlusion and impedance data. (A) Profiles of microcapillary occlusion in the 3- μ m to 10- μ m arrays shown as histograms for the tested RBC samples with 100% healthy RBCs, with 99% healthy

RBCs and 1% stiff RBCs, or with 98% healthy RBCs and 2% stiff RBCs. (B) The ROI of samples with 98% healthy RBCs and 2% stiff RBCs was significantly higher compared to that of samples with 99% healthy RBCs and 1% stiff RBCs or 100% healthy RBCs, and the ROI of samples with 99% healthy RBCs and 1% stiff RBCs was significantly higher compared to that of 100% healthy RBCs ($p < 0.05$, paired t-test). (C) Profiles of impedance change in those arrays shown as histograms for the tested RBC samples. (D) The REI of samples with 98% healthy RBCs and 2% stiff RBCs was significantly higher compared to that of samples with 99% healthy RBCs and 1% stiff RBCs or 100% healthy RBCs, and the REI of samples with 99% healthy RBCs and 1% stiff RBCs was significantly higher compared to that of 100% healthy RBCs ($p < 0.05$, paired t-test). (E) The REI significantly correlates with the ROI in the tested samples (PCC=0.987, $p < 0.0001$, $N=12$). ROI: RBC Occlusion Index. REI: RBC Electrical Impedance Index. PCC: Pearson correlation coefficient. Error bars represent standard deviation. $N=4$ for each group.

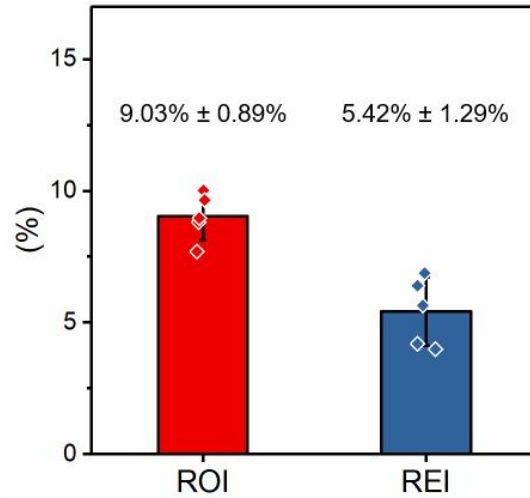


Fig. 3. Measurement reproducibility was assessed by repeatedly testing one RBC sample from a single healthy donor using five different devices. Shown are the ROI and REI results of the five repeats (mean \pm standard deviation). ROI: RBC Occlusion Index. REI: RBC Electrical Impedance Index. Error bars represent standard deviation.

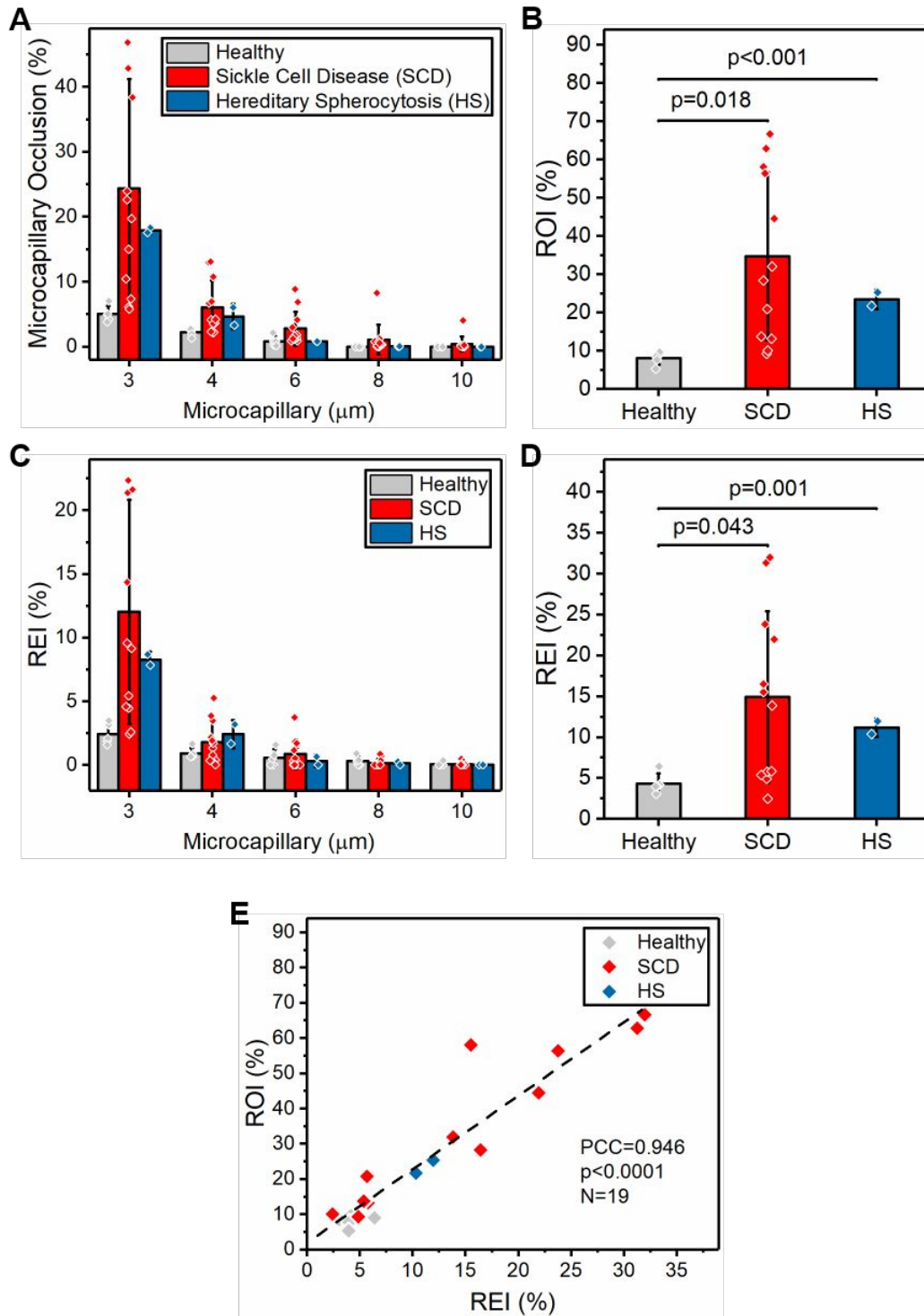


Fig. 4. Assessment of RBC deformability and microvascular occlusion in two common red cell disorders, sickle cell disease (SCD) and hereditary spherocytosis (HS). (A) Histograms of microcapillary occlusion for the tested RBC samples from healthy donors and subjects with SCD or HS. (B) The ROI of RBCs from

subjects with SCD or HS is significantly higher compared to that from healthy donors ($p < 0.05$, one-way ANOVA). (C) Histograms of impedance change for the tested RBC samples from healthy donors and subjects with SCD or HS. (D) The REI of RBCs from subjects with SCD or HS is also significantly higher compared to that from healthy donors ($p < 0.05$, one-way ANOVA). (E) The REI significantly correlates with the ROI in the tested samples ($PCC = 0.946$, $p < 0.0001$, $N = 19$). ROI: RBC Occlusion Index. REI: RBC Electrical Impedance Index. PCC: Pearson correlation coefficient. Error bars represent standard deviation. $N = 5$ for healthy, $N = 12$ for SCD, and $N = 2$ for HS.

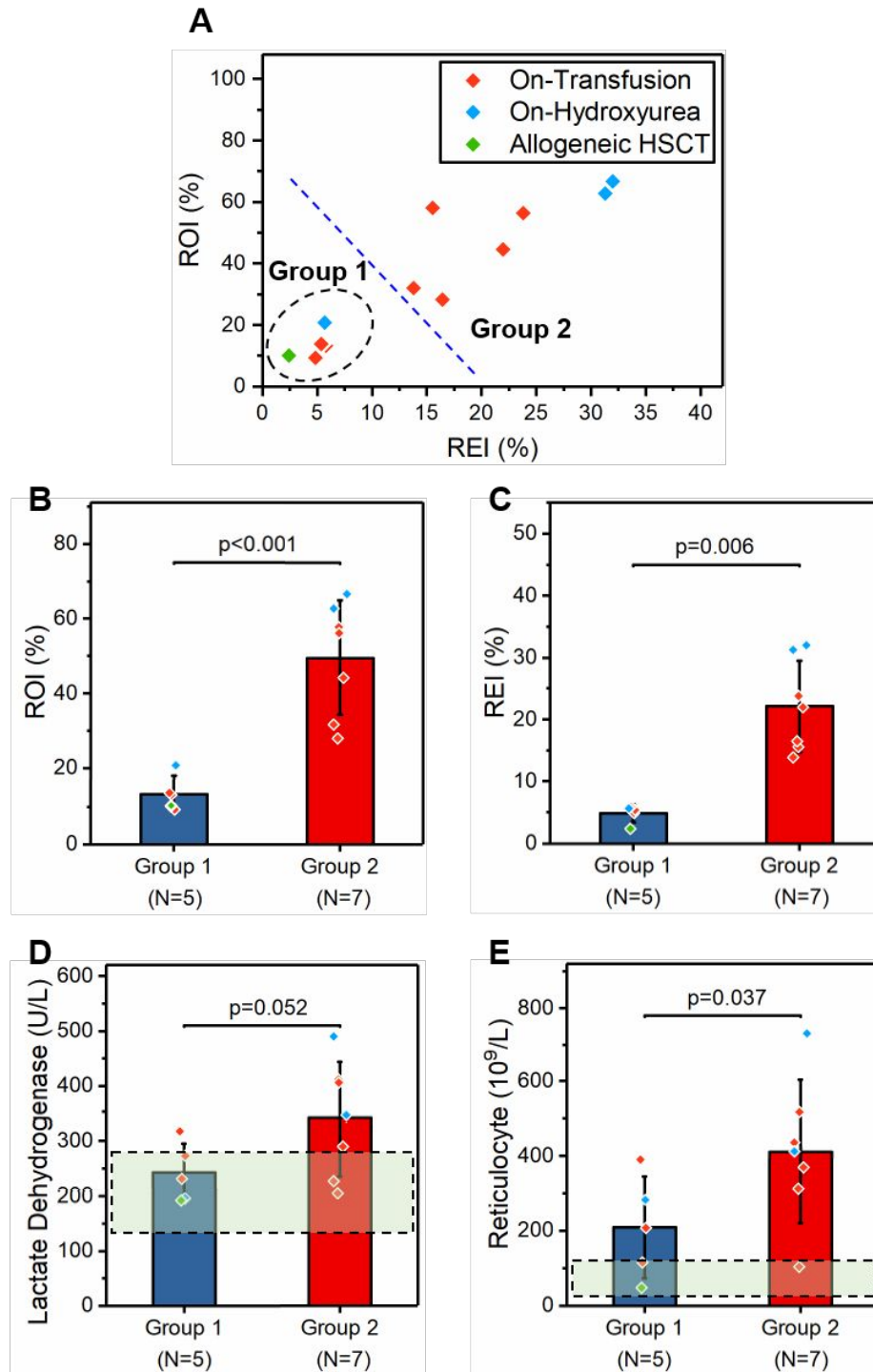


Fig. 5. Microfluidic electrical impedance assessment of RBC mediated microvascular occlusion as an in vitro therapeutic efficacy benchmark to assess the clinical outcome of treatments in SCD. (A) A subpopulation (Group 1, N=5) with distinct ROI and REI profiles compared to the rest (Group 2, N=7) was

identified. Group 1 subjects had significantly lower (B) ROI ($p < 0.001$, one-way ANOVA) and (C) REI ($p = 0.006$, Mann-Whitney) compared to Group 2 subjects. Moreover, Group 1 subjects had relatively lower (D) serum lactate dehydrogenase (LDH) levels ($p = 0.052$, Mann-Whitney) and (E) absolute reticulocyte counts (ARCs) ($p = 0.037$, Mann-Whitney) compared to Group 2 subjects. The dashed rectangular regions represent typical normal ranges for the given clinical parameters. HSCT: hematopoietic stem-cell transplantation. ROI: RBC Occlusion Index. REI: RBC Electrical Impedance Index. Error bars represent standard deviation.